Science of the Total Environment 906 (2024) 167382

Contents lists available at ScienceDirect

Science of the Total Environment

journal homepage: www.elsevier.com/locate/scitotenv

Unraveling the persistence of deep podzolized carbon: Insights from organic matter characterization

Ryan E. Champiny [a,*], Allan R. Bacon [a], Isabella D. Brush [a], Amy M. McKenna [b,c], Daniel J. Colopietro [a], Yang Lin [a]

[a] Department of Soil, Water, and Ecosystem Science, University of Florida, Gainesville, FL 32611, USA
[b] National Magnetic Field Laboratory, Florida State University, Tallahassee, FL 32310, USA
[c] Department of Soil and Crop Sciences, Colorado State University, Fort Collins, CO 80523, USA

HIGHLIGHTS

- DPC appears less refractory compared to overlying subsoil horizons.
- Reducing conditions caused by persistent water saturation influence DPC chemistry and stabilization.
- DPC C:N breaks with general trends in mineral subsoil C:N and is consistent with C:N of equatorial and hydromorphic podzols.

GRAPHICAL ABSTRACT

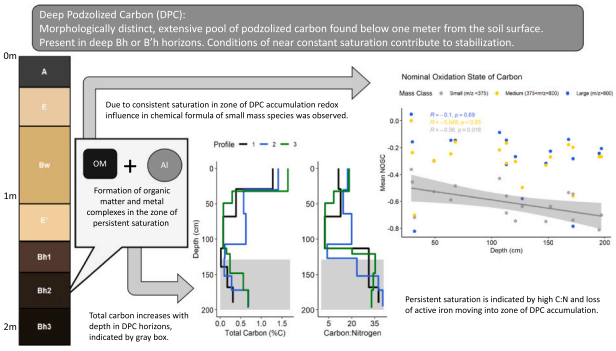

ARTICLE INFO

Editor: Jose Julio Ortega-Calvo

Keywords:
Podzolization
FT ICR-MS
Molecular characterization
Subsoil
Deep soil

ABSTRACT

Over a billion tons of terrestrial carbon (C) is stored in deep soils from the Southeastern Coastal Plain of the United States. While the size and extent of this pool, known as deep podzolized carbon (DPC), have been reported in recent studies, the stabilization mechanisms responsible for its persistence are unclear. The main hypothesis of DPC stabilization is that hydrology, specifically water table fluctuations in the phreatic zone, slow microbial degradation and promote C accumulation. This accounts for the characteristic properties and distribution of DPC and provides a mechanistic distinction between DPC and shallow podzolized C in the region's soils, however it has yet to be tested. We characterized the organic matter composition of the bulk and dissolved fractions of DPC using elemental analysis, solvent extraction, infrared spectroscopy, and high-resolution mass spectrometry. Consistent with past work, the majority of DPC organic matter was extractable by sodium pyrophosphate solution; the influence of metal association was also observable in the water extractable fraction of DPC with large species being preferentially removed and a low compound diversity compared to those from other horizons overlying DPC. Only water extractable species with low molecular mass (m/z < 375 Da) showed significant change in average nominal oxidation state of carbon (NOSC) values, indicative of oxygen-limitation influence on the processing of these species. Infrared spectroscopy revealed an increase in abundance of aliphatic (C-H:C-O) bonds relative to polysaccharide bonds with depth whereas aromatic (C=C:C-O) bonds decreased with depth in

* Corresponding author.
E-mail address: ryan.champiny@ufl.edu (R.E. Champiny).

https://doi.org/10.1016/j.scitotenv.2023.167382
Received 15 June 2023; Received in revised form 14 August 2023; Accepted 24 September 2023
Available online 27 September 2023

DPC relative to other subsurface horizons. Our work shows that DPC is significantly more refractory than overlying surface soil C, and yet slightly more labile than the subsoils above DPC. Together our results suggest that the maintenance of low redox conditions via persistent water saturation contributes to the stabilization and persistence of DPC.

1. Introduction

The soils of the Southeastern United States Coastal Plain contain over one billion tons of terrestrial carbon (C) in their deep horizons (Gonzalez et al., 2018). This subsoil C pool, known as deep podzolized carbon (DPC), has been reported for the better part of 50 years (Holzhey et al., 1975; Stone et al., 1993); however, only recently has a systematic evaluation of DPC been attempted (Bacon et al., 2020; Gonzalez et al., 2018). Given the large quantity of C stored in DPC horizons, as well as the interest in C sources and sinks due to global climate change, it is important to understand the nature and properties of DPC and the factors influencing its stability and persistence.

A general understanding of podzolization, the process in which organic matter (OM) is hydrologically transported into the subsoil where it accumulates with metals such as iron (Fe) and aluminum (Al) (Banik et al., 2014, 2016; Farmer, 1983; Lundström et al., 2000), as well as recent meta-analysis of podzolized C in the southeastern United States identifies metal association as an important component of DPC accumulation. More specifically, Gonzalez et al. (2018) evaluated 80 soil profiles with DPC across the southeastern United States and found that, on average, roughly 70 % of the C in DPC was metal associated, as indexed by sodium pyrophosphate extraction. Such metal association not only contributes to DPC accumulation by promoting the precipitation of organo-metal complexes, but it also protects against microbial decomposition given the relatively high energy costs associated with accessing it (Lundstrom et al., 1995; Marschner and Kalbitz, 2003; Schmidt et al., 2000; Wagai et al., 2013).

Bacon et al. (2020) hypothesized that hydrology, specifically water table fluctuations in the phreatic zone, also influences DPC accumulation. Their work demonstrated, at a regional scale, that a defining characteristic of DPC within a given soil profile is C concentration increases with depth through DPC (i.e., the shallowest reaches of DPC contain less C than deeper reaches of DPC). As landforms that accumulate DPC are endosaturated, the authors reasoned that this characteristic increase in C concentration with depth reflects the fact that the top of DPC is saturated less often than deeper portions of DPC. In other words, persistent water saturation is hypothesized to maintain low redox conditions and stabilize DPC in deeper portions of DPC. Similar explanations for development of Amazonian podzols have been put forward by Ishida et al. (2014) and have been more recently supported by Montes et al. (2023). While similar processes appear to be contributing to the persistence of these podzolized C pools, they are differentiated by their morphologies and C content. The Amazonian and equatorial soils display characteristics similar to vadose zone (shallow) podzolization, while the DPC studied here darkens with depth due to an increase in C content (Bacon et al., 2020; Ishida et al., 2014; Montes et al., 2011). While this reasoning does account for the characteristic properties and distribution of DPC and provide a mechanistic distinction between DPC and shallower pools of podzolized C which accumulate in the vadose zone of the region's soils, to date, it has yet to be tested.

Deep soil C persistence is also affected when the activities of microbial decomposers are limited by energy (Henneron et al., 2022). Deep mineral soils are globally characterized by low C:N ratios (< 15; higher N content per unit C), which approach that of microbial biomass (Rumpel and Kögel-Knabner, 2011). Due to low plant C input and the protection of OM by soil matrix in deep horizons, microbes have difficulty in acquiring energy that is necessary for growth and OM decomposition (Soong et al., 2020). Thus, low C:N ratios indicate energy limitation on microbial communities (Manzoni et al., 2012; Zechmeister-Boltenstern et al., 2015). Deep mineral soils with high C:N ratios have been reported in Andisols where plant-derived OM with high C:N ratios percolated from soil surface to subsoils through preferential flow paths and then stabilized by amorphous minerals (Kawahigashi et al., 2003; Marin-Spiotta et al., 2011). High C:N ratios have also been reported in a number of spodic horizons where water saturation and low redox conditions were hypothesized to promote the hydrolysis of N-rich OM and facilitate denitrification (Bardy et al., 2008; Do Nascimento et al., 2004; Ishida et al., 2014; Montes et al., 2023). Following the phreatic zone hypothesis, persistent water saturation would also support the accumulation of OM with high C:N ratios, especially in deeper portions of the DPC. Thus, organic matter quality (e.g., C:N ratio) can be indicative of the roles of different mechanisms in stabilizing OM in deep mineral soils (Jackson et al., 2017; Marschner and Kalbitz, 2003), however the role of these characteristics in stabilizing DPC and contributing to its accumulation in sandy soils of the Southeastern Coastal Plain have not yet been evaluated.

As the most mobile and actively cycling fraction of soil C, dissolved organic matter (DOM) can be particularly informative in revealing mechanisms underlying the persistence of DPC. Water-extractable organic carbon (WEOC) is a common index of DOM and dissolved organic carbon (DOC), and it is readily available for molecular characterization without the potential generation of artifacts that would occur in a more strongly alkaline or acidic extraction (Bahureksa et al., 2021; Guigue et al., 2014). While WEOC and DOC are not identical on a one-to-one basis, WEOC being a fraction that is extracted after agitation of soil in water over a set time period while DOC is collected in the field using equipment such as lysimeters, the WEOC fraction is taken to include the DOC fraction in addition to the C released from the destruction of aggregates (Chantigny, 2003). Because soils with primarily sandy textures have few micropores and consist mainly of macropores, the differences between WEOC and DOC are smaller compared to a more clayey soil (Chantigny, 2003; Zsolnay, 1996, 2003). Recent studies have shown that anoxic, oxygen limited, conditions lead to WEOC that is enriched in reduced species with relatively low nominal oxidation state of carbon (NOSC) values (Boye et al., 2017; Lin et al., 2021; Wilson and Tfaily, 2018). If water saturation in the phreatic zone was responsible for the persistence of DPC, then its WEOC would be characterized by a low NOSC value by enrichment of reduced species. The phreatic zone hypothesis also dictates that the NOSC value would decrease with increasing depth in the DPC horizons, as water saturation was more persistent in the deeper than in the upper portions of DPC.

To further understand the mechanisms responsible for DPC accumulation and persistence, we, for the first time, examine the chemical composition of both the bulk OM and DOM from DPC horizons. Specifically, our goal is to test the hypothesis that oxygen limitation associated with phreatic zone hydrology influences DPC stabilization, as suggested by Bacon et al. (2020). In support of this hypothesis, we expect to find the following: (1) Bulk soil organic matter from DPC will have higher C:N ratios than overlying horizons that reflect persistence water saturation and preferential removal of N. C:N ratios would also increase with increasing depth within DPC horizons. (2) The OM composition of DPC becomes increasingly labile with depth, reflecting the suppressed microbial processing imposed by the reducing conditions of the phreatic zone. (3) DOM from DPC will be enriched by low molecular mass, reduced organic species with low NOSC values compared to those from overlying horizons. The NOSC values of DOM will also decrease with increasing depth within DPC horizons, indicative of the more persistent saturation conditions in deeper portions of the DPC.

2. Materials and methods

2.1. Sample collection and site description

Soil samples were collected from the North Florida Research and Education Center, Live Oak, FL, where DPC has been identified and characterized by a past study (Bacon et al., 2020). Briefly, the soils sampled for this study have been mapped as the Leon fine sands series consociation and were formed in sandy marine sediments (United States Department of Agriculture (USDA), 2017). The field in which samples were taken was used as overflow bahiagrass (*Paspalum notatum*) pasture for occasional livestock grazing, with no addition of mineral fertilizer or other agricultural amendment apart from cow feces. Prior to conversion to agriculture the dominant ecosystem type ranged from sandhill longleaf pine (*Pinus palustrus*) savannah, to mixed flatwoods with increasing proximity to wetlands (United States Department of Agriculture (USDA), 2017). Soils were augered to the water table, around 80 cm beneath the soil surface, then cored using a JMC subsoil probe (3 cm diameter) with a plastic sheath liner to a depth of 2 m. Three soil profiles were sampled as replicates to capture potential spatial heterogeneity of DPC along a 60-m transect spaced 20-m apart (Supplemental Fig. A-1). A total of 20 samples were taken, one for each horizon to detect vertical changes in OM composition (Table 1). The horizons were differentiated based on moist color under natural light using the Munsell color chart. Texture did not vary significantly in the soil profiles, all of which fell within the loamy sand texture class. Soil pH was measured using an Accumet AB200 pH meter (Fisher) with soil suspended in a 1:1 ratio of water to air-dry soil. Three measurements were taken for each sample and the median pH value was recorded in Table 1.

2.2. Bulk soil analysis

For bulk analysis air-dry soils were sieved to 2 mm. Subsets of each sample were air-dried, ball-milled (8000D Mixer Mill, Spex SamplePrep), and then analyzed for total C and N via an elemental analyzer (ECS 4010, Costech). 0.5 g of air-dried soil from each sample were mixed with 30 mL of 0.1 M sodium pyrophosphate ($Na_4P_2O_7$) solution in acid-washed polypropylene (Falcon) centrifuge tubes. The soil-solution mixtures were shaken horizontally for 12 h, then centrifuged for 15 min at 6000 RPM on a Beckman model J2–21 centrifuge. Centrifuged solutions were vacuum filtered using Whatman #42 filter paper, glass funnels and vacuum flasks. A 1 mL subset of each sample was diluted to 8 mL with ultrapure (18.2 mΩ) water and analyzed on a Shimadzu TOC-L_{CSN} to determine organic C and N concentrations. Solutions were digested and then analyzed for Fe and Al concentration by the inductively coupled plasma technique (Lopez-Sangil and Rovira, 2013). Briefly, 25 mL solution was transferred to digestion tubes and digested on a hot block (Environmental Express) at 95 °C with sequential additions of 1 mL 65 % nitric acid (HNO_3) and 3 mL 30 % H_2O_2. Solutions remained on the hot block until they were both free of precipitate as well as transparent. Digestates were brought back to 35 mL volume using 0.01 M HNO_3 solution before ICP-OES analysis with blind duplicates for quality control.

Table 1
Index and general properties of samples taken at the North Florida Research and Extension Center in Suwannee County, FL.

Code	Profile	Horizon (USDA)	Depth (cm)	Wet color	pH
SV11	1	A	0–29	10YR 2/1	5.69
SV12	1	E	29–68	10YR 5/2	5.29
SV13	1	Bw	68–113	10YR 5/4	5.19
SV14	1	E'	113–139	10YR 7/1	5.40
SV15	1	Bh1	139–168	10YR 3/1	5.20
SV16	1	Bh2	168–190	10YR 2/1	5.15
SV21	2	A	0–30	10YR 2/1	5.55
SV22	2	E	30–64	10YR 5/2	5.37
SV23	2	Bw	64–107	10YR 4/3	5.10
SV24	2	E'	107–127	10YR 5/3	5.12
SV25	2	Bh1	127–152	7.5YR 4/2	5.51
SV26	2	Bh2	152–172	7.5YR 3/1	5.40
SV27	2	Bh3	172–195	10YR 2/1	5.16
SV31	3	A	0–32	10YR 2/1	5.75
SV32	3	E	32–49	10YR 5/2	5.00
SV33	3	Bw	49–113	10YR 5/4	4.77
SV34	3	E'	113–121	7.5YR 4/2	4.51
SV35	3	Bh1	121–148	7.5YR 3/1	4.97
SV36	3	Bh2	148–172	7.5YR 2.5/1	5.06
SV37	3	Bh3	172–197	10YR 2/1	4.89

2.3. Diffuse reflectance infrared Fourier transform spectroscopy (DRIFTS)

Ball-milled soil samples were analyzed with diffuse reflectance infrared Fourier transform spectroscopy (DRIFTS) to assess OM composition (Hall et al., 2018; Mainka et al., 2022). Samples were oven dried at 40 °C and homogenized with spectroscopy-grade KBr in a 1:20 ratio (soil:Kbr). Absorption was measured between 4000 and 400 cm^{-1} over 64 scans using a Nicolet iS50 FTIR spectrometer. Spectra were corrected against a background KBr sample and adjusted to remove the H_2O and CO_2 interference. We presented the ratios of peak regions that are well-documented to correspond to OM functional groups (Table 2). Specifically, we focused on four functional groups: aliphatic C—H bonds, carbonyl/carboxylic C═O bonds, aromatic C═C bonds, and polysaccharide C—O bonds. The peak regions centered around 2927 cm^{-1} (2943–2910 cm^{-1}) and 2853 cm^{-1} (2865–2840 cm^{-1}) were attributed to aliphatic C—H stretching and represented simple plant-derived OM, e.g., simple root exudates and carbohydrates (Mainka et al., 2022). The peak region centered around 1605 cm^{-1} (1640–1570 cm^{-1}) was attributed to a carbonyl/carboxylic C═O stretch of amides, quinones, and ketones with potential contribution from aromatic species (Hall et al., 2018; Parikh et al., 2014). We interpreted the peak region centered around 1529 cm^{-1} (1550–1508 cm^{-1}) as an aromatic C═C stretch that represents complex plant-derived OM, such as lignin and polyphenols (Calderón et al., 2013). Finally, we attributed the peak region centered around 1059 cm^{-1} (1071–1046 cm^{-1}) to the bending C—O bonds in carbohydrates. For each peak region, the absorbance peak area was integrated using a local baseline (Demyan et al., 2012). We calculated the ratios of C—H bonds, C═O bonds, and aromatic C═C bonds relative to the C—O bonds by considering the C—O bonds as an internal standard (Ellerbrock and Gerke, 2004; Kaiser et al., 2016). This normalization method provides a semi-quantitative approach to compare OM composition across samples with various matrix and C content (Lehmann et al., 2007; Ryals et al., 2014). Multiple pieces of evidence (sand size distributions (Bacon et al., 2020) and Cremeens and Mokma (1986) uniformity value) indicate no lithologic discontinuities occur within the profiles, which allows us to assume similar parent material and minerology for horizon comparisons.

Table 2
Selected infrared bands for DRIFT spectra.

Wavenumber (cm^{-1})	Vibration	Functional group	Reference
2927, 2853	C-H stretching	Aliphatics	Mainka et al., 2022
1605	C=O stretching	Amides, quinones, ketones, with potential aromatics. (Carbonyl/Carboxylic)	Parikh et al., 2014
1529	C=C stretching	Aromatic plant compounds	Calderón et al., 2013
1059	C-O bend	Carbohydrates (Polysaccharides)	Parikh et al., 2014

2.4. 21 Tesla Fourier transform ion cyclotron resonance – mass spectrometry (FT ICR-MS)

To prepare WEOC samples for FT ICR-MS analysis, 8 g of fresh soil were mixed with 40 mL of ultrapure (18.2 mΩ) water at a 1:5 ratio of soil to water (mass to volume) in acid-washed 50-mL polypropylene centrifuge tubes. The extracts were shaken for 1 h and then centrifuged for 15 min at 6000 RPM. The supernatant was filtered through pre-combusted glass microfiber filters (Whatman GF/F) on an acid-washed glass vacuum filtration kit. Concentrations of WEOC and total N were analyzed using a Shimadzu TOC-L_{CSN} with four-point calibration curves.

To remove metal and salt interference, WEOC samples were passed through solid-phase extraction (SPE) cartridges following a well-tested procedure (Dittmar et al., 2008; Li et al., 2018). Briefly, filtered water was added and passed through the SPE cartridges (Agilent Bond Elute PPL, 3-mL capacity) that had been pre-conditioned with HPLC-grade methanol (J. T. Baker). After rinsing the cartridges with pH 2 ultrapure water, WEOC samples were eluted from the cartridges with 6 mL of HPLC-grade methanol. The methanol was evaporated under N_2 gas to a final volume of 2 mL to reach a C load of approximately 300 μg C mL^{-1} methanol.

SPE extracts and procedural controls were sent to the National High Magnetic Field Lab in Tallahassee, FL for negative-ion microelectrospray ionization FT ICR-MS characterization (Emmett et al., 1998). Typical conditions for negative ion formation were: emitter voltage, −2.5–3.0 kV; S-lens RF level 45 %; and heated metal capillary temperature, 350 °C. SPE extracts were analyzed with a custom-built hybrid linear ion trap FT ICR mass spectrometer equipped with a 21 T superconducting solenoid magnet (Hendrickson et al., 2015; Smith et al., 2018). Ions were excited to *m/z* depended radius to maximize the dynamic range and number of observed mass spectral peaks (32–64 %), and excitation and detection were performed on the same pair of electrodes (Chen et al., 2014; Kaiser et al., 2013). The dynamically harmonized ICR cell in the 21 T FT ICR is operated with a 6 V trapping potential (Boldin and Nikolaev, 2011; Kaiser et al., 2013). Time-dominant transients of 3.1 were conditionally co-added and acquired with the Predator data station that handled excitation and detection only, initiated by a TTL trigger from the commercial Thermo data station, with 100 time-domain acquisitions averaged for all experiments (Blakney et al., 2011). Mass spectra were phase-corrected and internally calibrated with 10–15 highly abundant homologous series that span the entire molecular weight distribution based on the "walking" calibration method (Savory et al., 2011; Xian et al., 2010). Experimentally measured masses were converted from the IUPACE mass scale to the Kendrick mass scale for rapid identification of homologous series (Kendrick, 1963a). Peaks with signal magnitude >6-times the baseline root-mean-square level were exported to a peak list. Molecular formula assignments were performed within the bounds of $C_{1\text{-}100}H_{3\text{-}200}O_{1\text{-}30}$ $N_{0\text{-}4}S_{0\text{-}1}$ and ± 0.5 ppm error with PetroOrg© software (Corilo, 2014; McLafferty and Turecek, 1993). Species with relative abundance of ≥0.05 % were considered. Owing to the presence of alkylbenzene sulfonate peaks, we did not include sulfur (*S*)-containing species in subsequent analyses. Two samples from profile 1 (E' and B2 horizons) were discarded due to extremely low peak numbers, resulting in a total of 18 samples with FT ICR-MS data (Supplemental Fig. A-2). For all mass spectra, the achieved resolving power at *m/z* 400– 1,500,000–2,000,000, with between 10,000–20,000 assigned species with 25–80 ppb mass error for all assignments. Raw FT ICR-MS files, calibrated peak lists, and assigned elemental compositions are publicly available via the Open Science Framework.

2.5. Data analysis

The sampled soil horizons were categorized into three groups, surface (A), subsurface (E, B, and E'), and DPC (Bh1, Bh2, and Bh3) horizons (Table 1). Soil characteristics were compared among the three groups using one-way analysis of variance (ANOVA) followed by Tukey's honestly significant difference (HSD) tests. Soil profile was considered as a block factor in the ANOVA. Pearson's correlation was computed between soil characteristics and soil depth to assess the vertical trends in soil properties. Correlation analyses were also conducted in DPC and non-DPC horizons separately to explore the depth dependence of soil properties in both types of horizons.

Dividing the $Na_4P_2O_7$-extractable organic C content by that of the soil total C yields the percentage of metal-associated C present in each sample:

$$\text{Metal} - \text{Associated C}\% = Na - pyro\ C / Total\ C \times 100\% \quad (1)$$

Using the assigned chemical formulae from the FT ICR analysis, experimentally measured masses were converted from the International Union of Pure and Applied Chemistry (IUPAC) mass scale to the Kendrick mass scale for rapid identification of homologous series for each heteroatom class (i.e., species with the same C, H, N, O, and S content, differing only be degree of alkylation) (Hughey et al., 2001; Kendrick, 1963b). For each formula, NOSC value was calculated using the following formula (LaRowe and van Cappellen, 2011):

$$NOSC = 4 - \frac{4C + H - 2O - 3N - 2S + 5P - z}{C} \quad (2)$$

where *z* represents the net charge of the organic compound and *C, H, O, N, S,* and *P*, correspond to the number of the corresponding element contained in the species. Species formulae were also grouped into major biochemical compound classes (i.e., amino sugar, carbohydrate, condensed hydrocarbon, lignin, lipid, protein, tannin, unsaturated hydrocarbon, and other) following Kim et al. (2003).

For a set of formula characteristics (species mass and NOSC value), weighted mean values were calculated for each soil horizon using the formula:

$$C_{wm} = \frac{\sum(C_i \times A_i)}{\sum A_i} \quad (3)$$

where C_{wm} refers to the weighted mean of a formula characteristic, C_i is the characteristic's value for formula *i*, and A_i indicates its relative abundance. We classified all observed formulae into three mass classes following their multi-modal distribution (Supplemental Fig. A-3): large ($m/z > 600$), medium ($375 < m/z \leq 600$), and small ($m/z < 375$) (Roth et al., 2019). For each class of mass, species biochemistry, and heteroatom, percent abundance was calculated as the sum of relative abundance of that class divided by the sum of all abundances. To describe compound diversity, we also calculated the Gini-Simpson index (D_A) for each soil horizon (Jost, 2006; Mentges et al., 2017):

$$D_A = 1 - \sum A_i^2 \quad (4)$$

Using Pearson's correlations, we examined the depth distribution of the weighted means of formula characteristics, percent abundances of compound classes, and the Gini-Simpson index. All analyses were performed in R version 4.1.2. (R Core Team, 2021).

3. Results and discussion

3.1. Characteristic trends in metal and carbon content

In the A horizons, Na-pyro extractable Al (pyro-Al) averages 1.83 mg Al g^{-1} soil, decreasing with depth to an average of 0.71 mg Al g^{-1} soil in E' horizons, and then increasing through DPC where it averages 0.90, 1.39, and 2.63 mg Al g^{-1} soil in Bh1, Bh2, and Bh3 horizons respectively (Fig. 1b and c). Na-pyro extractable Fe (pyro-Fe) is relatively stable in soil material overlying DPC, averaging 0.92, 0.66, 0.84, and 0.19 mg Fe g^{-1}soil in A, E, Bw, and E' horizons respectively and then abruptly decreases near the top of DPC where it averages 0.05 mg Fe g^{-1}soil.

The trend of sodium pyrophosphate extractable Al described above is similar to the pattern of total carbon (Fig. 1). In the sampled profiles,

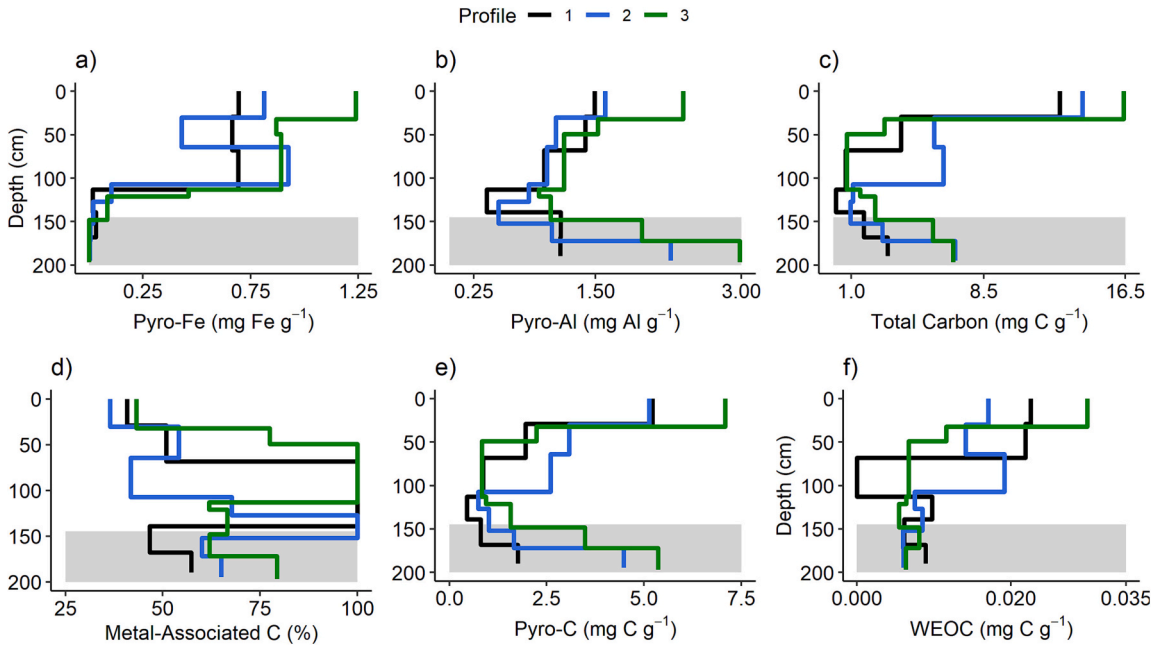

Fig. 1. Sodium pyrophosphate extractable ($Na_4P_2O_7$, Na-pyro) a) iron (pyro-Fe), b) aluminum (pyro-Al), c) total carbon (TC), d) Metal-Associated C (pyro-C/ total C x 100 %), sodium pyrophosphate extractable carbon (pyro-C) and f) water extractable organic carbon (WEOC) by sample profile. Horizons containing DPC are highlighted by the gray box.

total C attenuates sharply with depth from an average of 1.4 % in A horizons to an average of 0.09 % in E' horizons immediately overlying DPC, resulting in a negative correlation between total C and depth in horizons above DPC ($n = 12$, $r = -0.84$, $P < 0.001$). The decrease in total C reverses at the beginning of DPC in Bh1, where total C increases with depth from an average of 0.17 % in Bh1 horizons to an average of 0.38 % and 0.68 % in Bh2 and Bh3 horizons respectively. Correlation analysis also shows an increasing trend of total C with soil depth within DPC horizons ($n = 8$, $r = 0.77$, $P < 0.05$). This is a defining characteristic of DPC, one that is observed and reported region-wide (Bacon et al., 2020; Gonzalez et al., 2018). The total C and pyrophosphate extractable carbon fraction (pyro-C) (Fig. 1c and e) show similar general patterns across depth. The ratios of both TC and pyro-C to pyro-Al begin to converge in the DPC horizons starting at Bh1 (Supplemental Fig. A10). Both ratios decreased from the A horizons to the subsoils, reflecting the rapid depletion of C in subsurface relative to surface horizons. The depletion stabilizes and reverses beginning at Bh1, indicating an increase in C from the subsurface and into the DPC horizons. The percent metal-associated C (Fig. 1d) is shown to comprise >50 % of the total C in the DPC horizons, with the exception of Bh1 in profile 1. Percent metal C is used as an indication of podzolization, while lower percentages indicate surface C (Banik et al., 2016; Gonzalez et al., 2018). Unsurprisingly, Fig. 1f shows that the soil C in the Bh horizons are more strongly influenced by metal association.

The DPC horizons show a precipitous loss of Fe combined with increased Al content, showing that this C pool undergoes periods of prolonged saturation sufficient to promote Fe reduction and loss. Anoxic conditions lead to Fe reduction as oxygen is lost as the terminal electron acceptor for microbial activity. Reduced Fe is mobile in solution and so it is readily lost from the system, leaving behind Al-organic complexes. The relative abundance of Fe in comparison to Al can be indicative of the oxygen availability in DPC horizons (Banik et al., 2014; Lopes-Mazzetto et al., 2018). This pattern of extreme iron loss and OM-complexed aluminum preservation supports previous observations of metal content of DPC horizons in Bacon et al. (2020), Gonzalez et al. (2018), and is evidence that this carbon pool accumulates in the phreatic zone. In addition to favoring iron reduction, these reducing conditions can favor C accumulation by reducing microbial degradation and turnover of organic molecules (Boye et al., 2017).

3.2. Bulk analysis

Our results show that DPC has a unique chemical composition different from the C contained within overlying horizons. In the sample profiles, the ratio of total C:N decreases slightly with depth above DPC (averaging 15.6, 11.7, 8.3, and 12.1 in A, E, Bw, and E' horizons respectively) but then increases by almost three times with depth through DPC where it averages 29.9, 36.3, and 36.6 in Bh1, Bh2, and Bh3 horizons respectively (Fig. 2).

The high C:N ratio of DPC breaks with the global trend that mineral soil C:N ratios decrease with depth (Batjes, 2014), which has been attributed to the accumulation of microbially-derived OM (Rumpel and Kögel-Knabner, 2011). While, large C:N values in deep soil horizons can occur due to protection of the OM from microbial degradation, or via the loss of N under reducing conditions (Bardy et al., 2008; Do Nascimento et al., 2004). The C:N values observed in DPC indicate suppression of decomposition, such as through energy limitation and oxygen availability, within horizons containing DPC. This pattern suggests that the Southeastern Coastal Plain DPC is more similar to equatorial podzolized C, where consistent water saturation, or waterlogging, has been documented to be the primary driver of C persistence in these podzols Ishida et al., 2014; Kawahigashi et al., 2003; Merdy et al., 2021; Montes et al., 2023). Phreatic zone conditions, where soils are more likely to be consistently water-saturated and oxygen limited, would provide the necessary conditions to inhibit microbial activity or to promote the preferential loss of N. DPC in the Southeastern Coastal Plain may share similarities with equatorial and hydromorphic podzols, however it is still distinct due to characteristic increases in C content with depth.

The DRIFTS analysis of bulk soil samples shows distinct differences in OM composition between DPC and other horizons (Fig. 2). C-H:C-O attenuates sharply with depth from an average of 0.45 in A horizons to an average of 0.02 in E' horizons immediately overlying DPC. In DPC however, C-H:C-O tends to increase with depth from an average of 0.01 in Bh1 horizons to an average of 0.05 and 0.1 in Bh2 and Bh3 horizons respectively. Correlation analysis also shows that C-H:C-O first decreases with soil depth above DPC horizons ($n = 12$, $r = -0.76$, $P < 0.01$) and

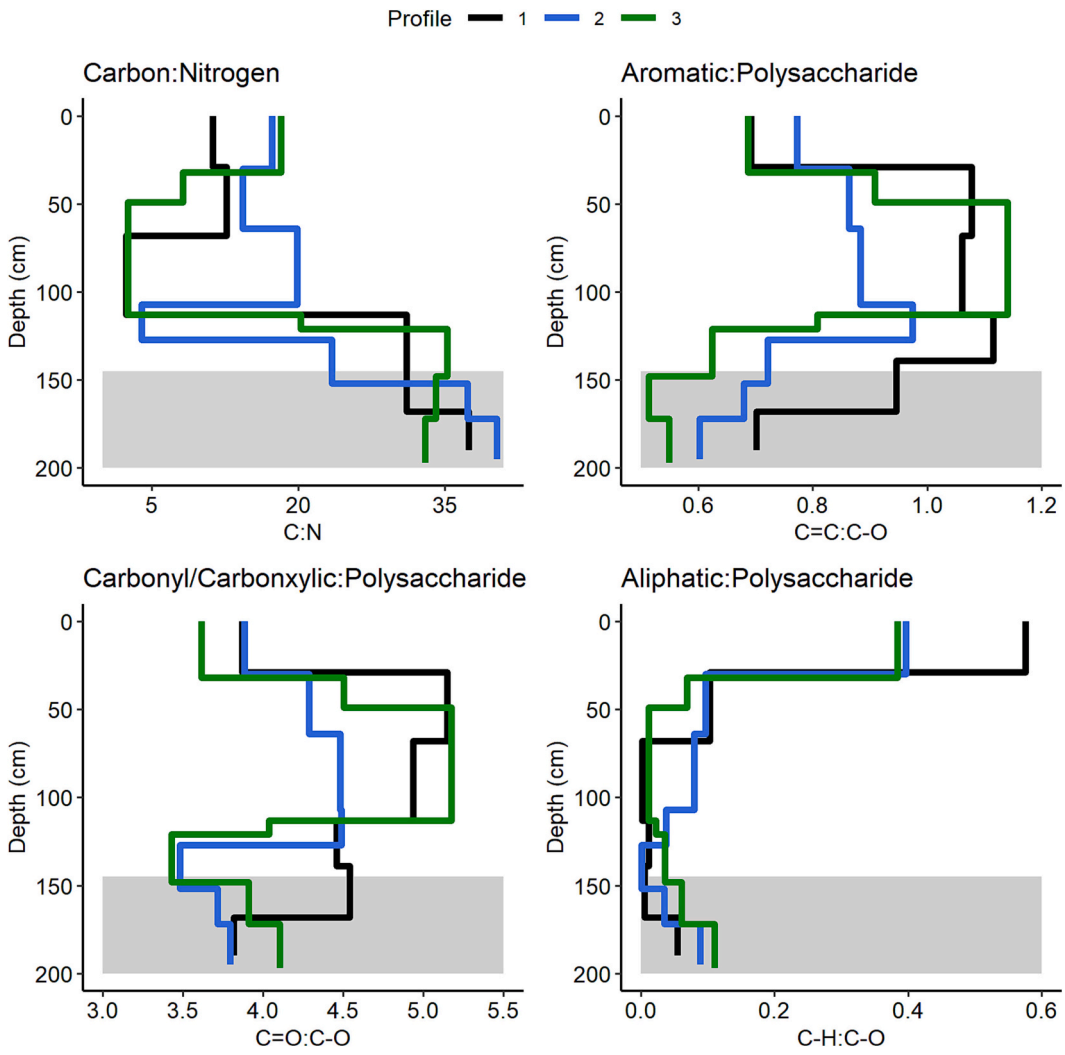

Fig. 2. Organic matter composition as revealed by bulk C:N and infrared spectroscopy (DRIFTS). C:N ratio based on bulk soil analysis, C=C:C-O the ratio of aromatic to polysaccharide functional groups, C=O:C-O the ratio of carbonyl/carboxylic to polysaccharide functional groups, C-H:C-O the ratio of aliphatic to polysaccharide functional groups. The shaded gray rectangle indicates the depth at which deep podzolized carbon horizons begin.

then increases with depth in DPC horizons ($n = 8$, $r = 0.80$, $P < 0.05$). Similar patterns occur in ratios comparing C-H:C=C and C-H:C=O, showing the robustness of the trend. Abundance of aliphatic compounds decrease with depth until reaching the top of DPC (Bh1) where they begin to increase with depth indicating that the top of DPC is relatively more refractory than the bottom of DPC. The C=O:C-O and C=C:C-O ratios were also distinct between the DPC and subsurface horizons. C=C:C-O averages 0.72 in A horizons and then increases in a stepwise pattern with depth to an average of 0.98, in E, Bw, and E' horizons. In DPC, C=C:C-O decreases with depth from an average of 0.76 in Bh1 horizons to an average of 0.63 and 0.58 in Bh2 and Bh3 horizons respectively. Abundance of aromatic compounds increase with depth until reaching DPC where they begin to decrease with depth, which indicates that top of DPC is relatively more refractory than the bottom of DPC. The depth distribution of C=O:C-O is similar to that of C=C:C-O in A, E, Bw, and E' horizons; averaging 3.79 in A and abruptly increasing to an average of 4.61 in E, Bw, and E' horizons. In DPC, C=O:C-O decreases to an average of 3.82 and 3.81 in Bh1 and Bh2 horizons, respectively, before increasing slightly to 3.95 in Bh3 horizons.

Infrared spectroscopy provides semiquantitative information on the relative abundances of OM functional groups, which in turn provide insight to the processes impacting SOM stability. The enrichment of aromatic C=C bonds (Fig. 2, Supplemental Fig. A-2) in the sampled subsurface horizons is generally interpreted as the accumulation of complex plant-derived species that are relatively refractory against microbial decomposition (Hall et al., 2018; Ryals et al., 2014). Following this explanation, the overall decline in aromatic C=C bonds with soil depth within the DPC horizons would suggest that DPC is less refractory than the C present in overlying subsurface horizons. This is in contrast to the trend observed for aliphatic functional groups, which are well-known to represent plant-derived, labile OM would be readily utilized by microbes as a food source, and tends to decrease in abundance from surface to subsoils (Calderón et al., 2013; Hall et al., 2018; Ryals et al., 2014). Unlike fresh plant-derived OM with high C:N ratios DRIFTS analysis reveals that DPC was depleted in the plant-derived aliphatic C—H bonds relative to surface soil, while also showing a small yet statistically significant increase in aliphatic functional groups, beginning at Bh1, relative to overlying subsurface horizons (Fig. 2). Decreases in C—H bonds compared to other functional groups are indicative of decomposition and transformation of the SOM (Hall et al., 2018; Ryals et al., 2014). The ratio of C—H functional groups to C—O, C=C and C=O increases with depth, indicating that the Bh1 is more degraded than Bh2 or Bh3. This pattern occurs regardless of denominator functional group and can be considered to be a robust indication of preservation against OM degradation (Fig. A-4). Combined with the observed loss of Fe with increasing Al content at depth, the high C:N ratios and

enrichment of aliphatic functional groups with depth within DPC horizons indicate reducing conditions which inhibit OM degradation.

3.3. Molecular characteristics of the WEOC

Above DPC, the concentration of WEOC decreases linearly with depth, averaging 0.023, 0.016, 0.008, and 0.008 mg C g^{-1} soil in A, E, Bw, and E' horizons respectively (Fig. 1, Supplemental Fig. A-9). Through DPC however, WEOC stabilizes at approximately 0.007 and is not depth dependent ($n = 7$, $r = 0.05$, $P > 0.05$). Although the WEOC concentrations of the horizons containing DPC remains stable with depth, the FT ICR-MS results revealed noticeable changes in DOM composition along soil profiles (Fig. 3). Mean species mass decreased significantly with soil depth ($n = 18$, $r = -0.57$, $P < 0.05$), as its value decreased from m/z 513 ± 7 on average in surface horizons to m/z 481 ± 5 in DPC horizons. The Gini-Simpson index of species diversity also decreased with depth (n = 18, $r = -0.61$, $P < 0.01$). This relationship was robust even after removing a potential outlier (Bh3 from profile 2; $n = 17$, $r = -0.56$, P < 0.05). However, neither the heteroatom class nor the functional group composition showed any obvious trends along soil profiles (Supplemental Figs. A-6 and A-7), and the DOM composition remained consistent. This could be due in part to ionization suppression that occurs in negative-ion electrospray of DOM, and future studies should target different ionization modes to more completely probe DPC composition (Roth et al., 2022). Mean NOSC was negatively correlated with depth, however there was not a significant decrease (P > 0.05) in mean NOSC value with increasing depth.

The vertical trend in species mass is better observed when all species were grouped into three mass classes (Fig. 4). Medium species (m/z: 375–600) increased in abundance with depth (n = 18, $r = 0.59$, P < 0.01), while the abundance of large species ($m/z > 600$) decreased with depth (n = 18, $r = -0.7$, P < 0.01). Small species ($m/z < 375$) showed no significant change in abundance with depth. When broken into groups based on species mass, only species with small molecular mass showed a significant decline in NOSC value with increasing depth (n = 18, $r = -0.56$, P < 0.05). In contrast, the mean NOSC of large- and medium-sized species decreased slightly with depth, however the change was not significant (both P > 0.05).

Reduced species with low NOSC values are expected to be preserved against microbial degradation under anoxic conditions as microbes select species with higher NOSC values (Keiluweit et al., 2016; LaRowe and van Cappellen, 2011). This trend is due to the thermodynamic prediction that the oxidation of reduced OM does not generate sufficient energy to support microbial life when coupled with alternative electron acceptors. To test the prediction that DPC chemistry is influenced by reducing conditions nominal oxidation state of carbon (NOSC) values were calculated from the chemical formulae of OM species. Only species with small molecular mass showed a significant vertical trend, which suggests a selective pressure driving the chemical composition of these species. Larger mass species tend to require more energy or enzyme input for degradation to occur, thus the trends seen in these profiles show a preferential utilization of available OM species.

The decline in mean species mass with soil depth is likely also influenced by metal protection of OM, as Al and Fe oxides have been shown to preferentially form complexes with relatively large DOM in past FT ICR-MS studies (Galindo and del Nero, 2014; Ye et al., 2020). This trend diverges from past studies that reported increasing compound size with soil depth as a key signature of microbial processing of DOM as species of low molecular mass are degraded and larger species are produced (Roth et al., 2019; Ye et al., 2020). During the podzolization process, microbes can interrupt organo-metal complexes to access low molecular weight OM; large OM species are then able to capture and form complexes with the metal ions, also causing a decline in compound diversity (Buurman and Jongmans, 2005; Lundstrom et al., 1995). Thus, our results suggest that metal association helps to shape DPC chemistry by preferentially retaining large dissolved species while smaller species

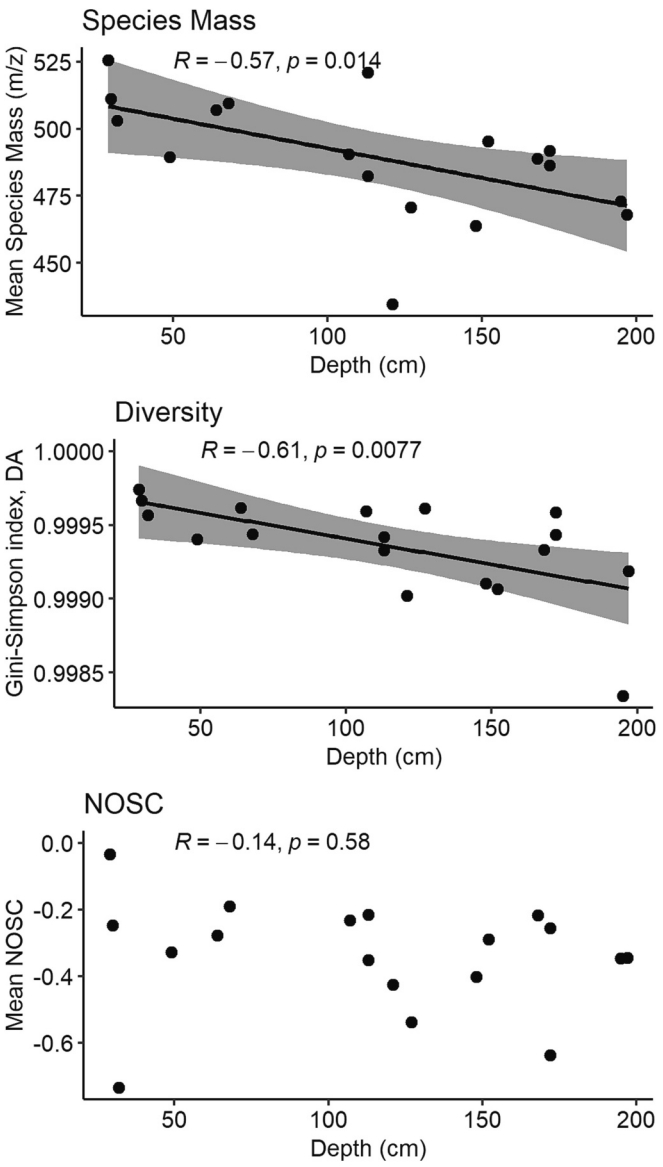

Fig. 3. FT ICR-MS organic matter characterization. A) Mean compound mass (m/z), B) Gini-Simpson index, and C) mean NOSC value as a function of depth for all identified compounds from the FT ICR-MS analysis. Higher Gini-Simpson index indicates higher compound diversity. R indicates Pearson's correlation coefficient, and p indicates its significance. Gray boxes indicate 95 % confidence intervals.

were available for microbial use, resulting in the NOSC trend.

The decreased diversity observed in the soil profiles might have implied a long residence time, or slow turnover rate, for DPC. In a recent study, soil OM was found to decrease in diversity as it persists through time (Jones et al., 2023). While radiocarbon dating records of DPC are extremely limited, the single radiocarbon estimate of DPC age is approximately 14 kyr (Bolivar, 2000), which is consistent with our interpretation. Together, our data on species mass, NOSC values, and diversity all support our hypothesis that water saturation plays a crucial role in enabling more persistent DPC towards deeper soil profiles.

Further research exploring molecular characteristics of DPC from different ecosystems and land management areas, utilizing a more diverse array of solvents, will provide a more complete picture of the chemical characteristics of this subsoil C pool. While WEOC is accepted as the most mobile fraction of soil C, it comprises only a small percentage of the total. The use of targeted or stronger extractants can provide a more extensive look into the composition of DPC, allowing the

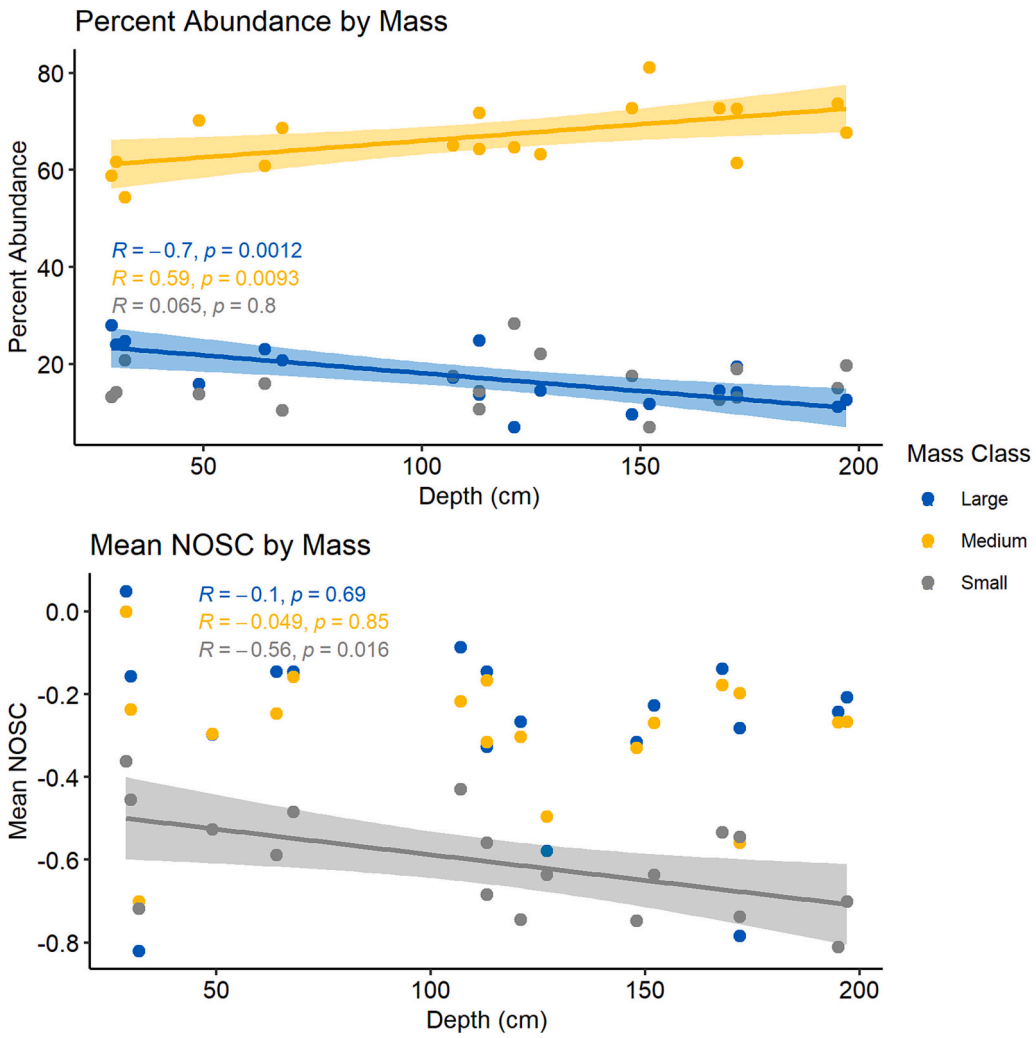

Fig. 4. FT ICR-MS characterization by mass class. A) Organic matter species mass class abundance by depth and b) NOSC value distribution of the three mass classes by depth. Species size classes were assigned based on natural *m/z* ratio distribution in the data (Supplemental Fig. A-1). R indicates Pearson's correlation coefficient, and p indicates its significance. Colored boxes indicate 95 % confidence intervals.

scientific community to further explore questions concerning C source and composition. Comparisons between DOC, cold WEOC, and hot WEOC using molecular characterization techniques such as ultra-high resolution mass spectrometry would also be worthy of investigation to examine differences in these dissolved fractions in both DPC and soils in general. Given the large quantity of C stored in DPC horizons, as well as their extent in the Southeastern Coastal Plain, understanding the factors influencing DPC persistence will provide better insight into the C cycling processes of the region's subsoils.

DPC persistence, like the persistence of all soil C, is a product of the interaction of intrinsic characteristics and external environmental factors of the regions in which it forms (Dungait et al., 2012). As we have noted here, the chemical fingerprint of phreatic hydrology as a stabilizing factor for this subsoil C is apparent based on the trends in OM-associated metals, DRIFTS, and FT-ICR results. Because persistent saturation and the high anaerobic cost of microbial respiration are stabilizing factors for DPC, land management decisions or climatic phenomena which impact these factors will likely have a strong subsequent effect on this C pool. Reduction in water level due to drainage control or altered rainfall patterns could reduce saturation of DPC and expose it to microbial degradation. This would likely release C from this extensive soil C pool, subsequently feedbacking back to climate change.

4. Conclusion

Here we combined bulk analysis methods, chemical extraction, and molecular characterization techniques to analyze the composition of deep podzolized carbon and provide insight on the factors contributing to its persistence. The results reported here highlight the complexity of this subsoil C and support the phreatic zone hypothesis of stabilization. There is a distinct increase in C:N ratio in DPC that distinguishes it from other subsoil C pools, and a loss of OM-associated Fe paired with an increase in OM-associated Al as depth increases. This metal trend implies a reducing environment consistent with phreatic conditions, which preserves carbon by increasing the energetic cost of microbial respiration. DRIFTS shows that DPC is more labile than C in overlying horizons, yet less refractory than surface soil. FTICR showed a decreasing trend in the NOSC value of small WEOC species whereas medium and large species did not show significant trends, implying that the reducing conditions drive selection by microbes for species that provide higher energetic return. Together, these findings demonstrate that DPC is a relatively stable C pool so long as the microbial community is unable to interrupt the Al-OM complexes which comprise DPC.

Supplementary data to this article can be found online at https://doi.org/10.1016/j.scitotenv.2023.167382.

CRediT authorship contribution statement

The authors contributed to this work in the following ways: Ryan E. Champiny (Conceptualization, Investigation, Methodology, Data Curation, Visualization, Formal analysis, Writing- Original Draft, Editing.); Allan R. Bacon (Writing- Review & Editing, Funding Acquisition for FT ICR-MS), Isabella D. Brush (Investigation), Amy M. McKenna (Investigation, Methodology for FT ICR-MS), Daniel J. Colopietro (Funding Acquisition for FT ICR-MS), Yang Lin (Conceptualization, Funding Acquisition, Methodology, Supervision, Visualization, Writing- Review & Editing).

Declaration of competing interest

The authors declare that they have no known competing financial interests or personal relationships that could have appeared to influence the work reported in this paper.

Data availability

Upon acceptance, FT ICR-MS data will be made available to the public at https://osf.io/az8gk/ and other data at https://zenodo.org/record/8384286.

Acknowledgements

We thank the staff at the Suwannee Valley Research and Extension Center for access to the research sites; Gary Scheiffele from The Herbert Wertheim College of Engineering's Research Service Centers for his guidance and support for the DRIFTS analysis; Swarnali Mahmood and Wendy Griffin for assistance with refining laboratory protocols; and Dr. Kanika Sharma Inglett for her comments on an earlier version of the manuscript. We also thank the associate editor and two anonymous reviewers for their helpful comments.

Funding sources

This work is supported by a U.S. Department of Agriculture Hatch grant FLA-SWS-006103 to YL. A portion of this work was performed at the National High Magnetic Field Laboratory, which is supported by National Science Foundation Division of Chemistry and Division of Materials Research through Cooperative Agreement No. DMR-1644779 and the State of Florida. Partial support came from the Biogeochemistry Fellowship for Masters students through the Wetland Biogeochemistry Lab at the University of Florida.

References

Bacon, A.R., Gonzalez, Y.N., Anderson, K.R., 2020. Morphologic and hydrologic distinctions between shallow and deep podzolized carbon in the southeastern United States Coastal Plain. Geoderma 361. https://doi.org/10.1016/j.geoderma.2019.114007.

Bahureksa, W., Tfaily, M.M., Boiteau, R.M., Young, R.B., Logan, M.N., McKenna, A.M., Borch, T., 2021. Soil organic matter characterization by Fourier transform ion cyclotron resonance mass spectrometry (FTICR MS): a critical review of sample preparation, analysis, and data interpretation. Environ. Sci. Technol. 55, 9637–9656. https://doi.org/10.1021/acs.est.1c01135.

Banik, C., Harris, W.G., Ellis, R., Hurt, W., Balboa, S., 2014. Relations of iron, aluminum, and carbon along transitions from Udults to Aquods. Geoderma 226–227, 332–339. https://doi.org/10.1016/J.GEODERMA.2014.03.016.

Banik, C., Harris, W.G., Ogram, A.v., Nair, V.D., 2016. Carbon, iron, and aluminum responses to controlled water table fluctuations in sandy soil material. J. Soil. Sediment. 16, 2449–2457. https://doi.org/10.1007/s11368-016-1444-z.

Bardy, M., Fritsch, E., Derenne, S., Allard, T., do Nascimento, N.R., Bueno, G.T., 2008. Micromorphology and spectroscopic characteristics of organic matter in waterlogged podzols of the upper Amazon basin. Geoderma 145, 222–230. https://doi.org/10.1016/j.geoderma.2008.03.008.

Batjes, N.H., 2014. Total carbon and nitrogen in the soils of the world. Eur. J. Soil Sci. 65, 10–21. https://doi.org/10.1111/EJSS.12114_2.

Blakney, G.T., Hendrickson, C.L., Marshall, A.G., 2011. Predator data station: a fast data acquisition system for advanced FT-ICR MS experiments. Int. J. Mass Spectrom. 306, 246–252. https://doi.org/10.1016/j.ijms.2011.03.009.

Boldin, I.A., Nikolaev, E.N., 2011. Fourier transform ion cyclotron resonance cell with dynamic harmonization of the electric field in the whole volume by shaping of the excitation and detection electrode assembly. Rapid Commun. Mass Spectrom. 25, 122–126. https://doi.org/10.1002/rcm.4838.

Bolivar, J.G.P., 2000. The Genesis Of Carbon Sequestration In Subtropical Spodosols (doctoral dissertation). Retrieved from George A. Smathers Library. https://ufdcimages.uflib.ufl.edu/UF/00/10/08/16/00001/thesis2.PDF.

Boye, K., Noël, V., Tfaily, M.M., Bone, S.E., Williams, K.H., Bargar, J.R., Fendorf, S., 2017. Thermodynamically controlled preservation of organic carbon in floodplains. Nat. Geosci. 10, 415–419. https://doi.org/10.1038/ngeo2940.

Buurman, P., Jongmans, A.G., 2005. Podzolisation and soil organic matter dynamics. Geoderma 125, 71–83. https://doi.org/10.1016/j.geoderma.2004.07.006.

Calderón, F., Haddix, M., Conant, R., Magrini-Bair, K., Paul, E., 2013. Diffuse-reflectance Fourier-transform mid-infrared spectroscopy as a method of characterizing changes in soil organic matter. Soil Sci. Soc. Am. J. 77, 1591–1600. https://doi.org/10.2136/sssaj2013.04.0131.

Chantigny, M.H., 2003. Dissolved and water-extractable organic matter in soils: a review on the influence of land use and management practices. Geoderma 113, 357–380. https://doi.org/10.1016/S0016-7061(02)00370-1.

Chen, T., Beu, S.C., Kaiser, N.K., Hendrickson, C.L., 2014. Note: optimized circuit for excitation and detection with one pair of electrodes for improved Fourier transform ion cyclotron resonance mass spectrometry. Rev. Sci. Instrum. 85, 066107 https://doi.org/10.1063/1.4883179.

Corilo, Y.E., 2014. PetroOrg Software.

Cremeens, D.L., Mokma, D.L., 1986. Argillic horizon expression and classification in the soils of two Michigan Hydrosequences. Soil Sci. Soc. Am. J. 50, 1002–1007. https://doi.org/10.2136/sssaj1986.03615995005000040034x.

Demyan, M.S., Rasche, F., Schulz, E., Breulmann, M., Müller, T., Cadisch, G., 2012. Use of specific peaks obtained by diffuse reflectance Fourier transform mid-infrared spectroscopy to study the composition of organic matter in a Haplic Chernozem. Eur. J. Soil Sci. 63, 189–199. https://doi.org/10.1111/j.1365-2389.2011.01420.x.

Dittmar, T., Koch, B., Hertkorn, N., Kattner, G., 2008. A simple and efficient method for the solid-phase extraction of dissolved organic matter (SPE-DOM) from seawater. Limnol Oceanogr Methods 230–235.

Do Nascimento, N.R., Bueno, G.T., Fritsch, E., Herbillon, A.J., Allard, Th., Melfi, A.J., Astolfo, R., Boucher, H., Li, Y., 2004. Podzolization as a deferralitization process: a study of an Acrisol-Podzol sequence derived from Palaeozoic sandstones in the northern upper Amazon Basin. Eur. J. Soil Sci. 55, 523–538. https://doi.org/10.1111/j.1365-2389.2004.00616.x.

Dungait, J.A.J., Hopkins, D.W., Gregory, A.S., Whitmore, A.P., 2012. Soil organic matter turnover is governed by accessibility not recalcitrance. Glob. Chang. Biol. 18, 1781–1796. https://doi.org/10.1111/j.1365-2486.2012.02665.x.

Ellerbrock, R.H., Gerke, H.H., 2004. Characterizing organic matter of soil aggregate coatings and biopores by Fourier transform infrared spectroscopy. Eur. J. Soil Sci. 55, 219–228. https://doi.org/10.1046/j.1365-2389.2004.00593.x.

Emmett, M.R., White, F.M., Hendrickson, C.L., Shi, S.D.-H., Marshall, A.G., 1998. Application of micro-electrospray liquid chromatography techniques to FT-ICR MS to enable high-sensitivity biological analysis. J. Am. Soc. Mass Spectrom. 9, 333–340. https://doi.org/10.1016/S1044-0305(97)00287-0.

Farmer, V.C., 1983. Genesis of humus B horizons in hydromorphic humus Podzols. Nature 304, 342–344.

Galindo, C., del Nero, M., 2014. Molecular level description of the sorptive fractionation of a fulvic acid on aluminum oxide using electrospray ionization Fourier Transform Mass Spectrometry. Environ. Sci. Technol. 48, 7401–7408. https://doi.org/10.1021/es501465h.

Gonzalez, Y.N., Bacon, A.R., Harris, W.G., 2018. A billion tons of unaccounted for carbon in the southeastern United States. Geophys. Res. Lett. 45, 7580–7587. https://doi.org/10.1029/2018GL077540.

Guigue, J., Mathieu, O., Lévêque, J., Mounier, S., Laffont, R., Maron, P.A., Navarro, N., Chateau, C., Amiotte-Suchet, P., Lucas, Y., 2014. A comparison of extraction procedures for water-extractable organic matter in soils. Eur. J. Soil Sci. 65, 520–530. https://doi.org/10.1111/EJSS.12156.

Hall, S.J., Berhe, A.A., Thompson, A., 2018. Order from disorder: do soil organic matter composition and turnover co-vary with iron phase crystallinity? Biogeochemistry 140, 93–110. https://doi.org/10.1007/s10533-018-0476-4.

Hendrickson, C.L., Quinn, J.P., Kaiser, N.K., Smith, D.F., Blakney, G.T., Chen, T., Marshall, A.G., Weisbrod, C.R., Beu, S.C., 2015. 21 tesla Fourier transform ion cyclotron resonance mass spectrometer: a National Resource for ultrahigh resolution mass analysis. J. Am. Soc. Mass Spectrom. 26, 1626–1632. https://doi.org/10.1007/s13361-015-1182-2.

Henneron, L., Balesdent, J., Alvarez, G., Barré, P., Baudin, F., Basile-Doelsch, I., Cécillon, L., Fernandez-Martinez, A., Hatté, C., Fontaine, S., 2022. Bioenergetic control of soil carbon dynamics across depth. Nat. Commun. 13, 7676. https://doi.org/10.1038/s41467-022-34951-w.

Holzhey, C.S., Daniels, R.B., Gamble, E.E., 1975. Thick Bh horizons in the North Carolina Coastal Plain: II. Physical and chemical properties and rates of organic additions from surface sources. Soil Science Society of America Journal 39, 1182–1187. https://doi.org/10.2136/SSSAJ1975.03615995003900060040X.

Hughey, C.A., Hendrickson, C.L., Rodgers, R.P., Marshall, A.G., Qian, K., 2001. Kendrick mass defect spectrum: a compact visual analysis for ultrahigh-resolution broadband mass spectra. Anal. Chem. 73, 4676–4681. https://doi.org/10.1021/ac010560w.

Ishida, D.A., Montes, C.R., Lucas, Y., Pereira, O.J.R., Merdy, P., Melfi, A.J., 2014. Genetic relationships between ferralsols, podzols and white kaolin in Amazonia. Eur. J. Soil Sci. 65, 706–717. https://doi.org/10.1111/ejss.12167.

Jackson, R.B., Lajtha, K., Crow, S.E., Hugelius, G., Kramer, M.G., Piñeiro, G., 2017. The ecology of soil carbon: pools, vulnerabilities, and biotic and abiotic controls. Annu. Rev. Ecol. Evol. Syst. 48, 419–445. https://doi.org/10.1146/annurev-ecolsys-112414-054234.

Jones, A.R., Dalal, R.C., Gupta, V.V.S.R., et al., 2023. Molecular complexity and diversity of persistent soil organic matter. Soil Biol. Biochem. 184, 109061 https://doi.org/10.1016/j.soilbio.2023.109061.

Jost, L., 2006. Entropy and diversity. Oikos 113, 363–375. https://doi.org/10.1111/j.2006.0030-1299.14714.x.

Kaiser, M., Zederer, D.P., Ellerbrock, R.H., Sommer, M., Ludwig, B., 2016. Effects of mineral characteristics on content, composition, and stability of organic matter fractions separated from seven forest topsoils of different pedogenesis. Geoderma 263, 1–7. https://doi.org/10.1016/j.geoderma.2015.08.029.

Kaiser, N.K., McKenna, A.M., Savory, J.J., Hendrickson, C.L., Marshall, A.G., 2013. Tailored ion radius distribution for increased dynamic range in FT-ICR mass analysis of complex mixtures. Anal. Chem. 85, 265–272. https://doi.org/10.1021/ac302678v.

Kawahigashi, M., Sumida, H., Yamamoto, K., 2003. Seasonal changes in organic compounds in soil solutions obtained from volcanic ash soils under different land uses. Geoderma 113, 381–396. https://doi.org/10.1016/S0016-7061(02)00371-3.

Keiluweit, M., Nico, P.S., Kleber, M., Fendorff, S., 2016. Are oxygen limitations under recognized regulators of organic carbon turnover in upland soils? Biogeochemistry 127, 157–171. https://doi.org/10.1007/s10533-015-0180-6.

Kendrick, E., 1963a. A mass scale based on CH2 = 14.0000 for high resolution mass spectrometry of organic compounds. Anal. Chem. 35, 2146–2154. https://doi.org/10.1021/AC60206A048/ASSET/AC60206A048.FP.PNG_V03.

Kendrick, Edward, 1963b. A mass scale based on CH $_2$ = 14.0000 for high resolution mass spectrometry of organic compounds. Anal. Chem. 35, 2146–2154. https://doi.org/10.1021/ac60206a048.

Kim, S., Kramer, R.W., Hatcher, P.G., 2003. Graphical method for analysis of ultrahigh-resolution broadband mass spectra of natural organic matter, the Van Krevelen diagram. Anal. Chem. 75, 5336–5344.

LaRowe, D.E., van Cappellen, P., 2011. Degradation of natural organic matter: a thermodynamic analysis. Geochim. Cosmochim. Acta 75, 2030–2042. https://doi.org/10.1016/J.GCA.2011.01.020.

Lehmann, J., Kinyangi, J., Solomon, D., 2007. Organic matter stabilization in soil microaggregates: implications from spatial heterogeneity of organic carbon contents and carbon forms. Biogeochemistry 85, 45–57. https://doi.org/10.1007/s10533-007-9105-3.

Li, X.M., Sun, G.X., Chen, S.C., Fang, Z., Yuan, H.Y., Shi, Q., Zhu, Y.G., 2018. Molecular Chemodiversity of dissolved organic matter in Paddy soils. Environ. Sci. Technol. 52, 963–971. https://doi.org/10.1021/acs.est.7b00377.

Lin, Y., Campbell, A.N., Bhattacharyya, A., DiDonato, N., Thompson, A.M., Tfaily, M.M., Nico, P.S., Silver, W.L., Pett-Ridge, J., 2021. Differential effects of redox conditions on the decomposition of litter and soil organic matter. Biogeochemistry 154 (1), 1–15. https://doi.org/10.1007/S10533-021-00790-Y.

Lopes-Mazzetto, J.M., Buurman, P., Schellekens, J., et al., 2018. Soil morphology related to hydrology and degradation in tropical coastal podzols (SE Brazil). Catena 162, 1–13. https://doi.org/10.1016/J.CATENA.2017.11.007.

Lopez-Sangil, L., Rovira, P., 2013. Sequential chemical extractions of the mineral-associated soil organic matter: an integrated approach for the fractionation of organo-mineral complexes. Soil Biol. Biochem. 62, 57–67. https://doi.org/10.1016/j.soilbio.2013.03.004.

Lundstrom, U.S., Breemen, N., Jonmans, A.G., 1995. Evidence for microbial decomposition of organic acids during podzolization. Eur. J. Soil Sci. 46, 489–496. https://doi.org/10.1111/j.1365-2389.1995.tb01345.x.

Lundström, U.S., van Breemen, N., Bain, D., 2000. The podzolization process. A review. Geoderma 94, 91–107. https://doi.org/10.1016/S0016-7061(99)00036-1.

Mainka, M., Summerauer, L., Wasner, D., Garland, G., Griepentrog, M., Berhe, A.A., Doetterl, S., 2022. Soil geochemistry as a driver of soil organic matter composition: insights from a soil chronosequence. Biogeosciences 19, 1675–1689. https://doi.org/10.5194/bg-19-1675-2022.

Manzoni, S., Taylor, P., Richter, A., Porporato, A., Ågren, G.I., 2012. Environmental and stoichiometric controls on microbial carbon-use efficiency in soils. New Phytol. https://doi.org/10.1111/j.1469-8137.2012.04225.x.

Marin-Spiotta, E., Chadwick, O.A., Kramer, M., Carbone, M.S., 2011. Carbon delivery to deep mineral horizons in Hawaiian rain forest soils. J. Geophys. Res. 116, G03011 https://doi.org/10.1029/2010JG001587.

Marschner, B., Kalbitz, K., 2003. Controls of bioavailability and biodegradability of dissolved organic matter in soils. Geoderma 113, 211–235. https://doi.org/10.1016/S0016-7061(02)00362-2.

McLafferty, F.W., Turecek, F., 1993. Interpretation of Mass Spectra, Fourth. ed. University Science Books, Mill Valley, California. https://doi.org/10.1002/bms.1200230614.

Mentges, A., Feenders, C., Seibt, M., Blasius, B., Dittmar, T., 2017. Functional molecular diversity of marine dissolved organic matter is reduced during degradation. Front Mar Sci 4. https://doi.org/10.3389/fmars.2017.00194.

Merdy, P., Lucas, Y., Coulomb, B., Melfi, A.J., Montes, C.R., 2021. Soil organic carbon mobility in equatorial podzols: soil column experiments. SOIL 7, 585–594. https://doi.org/10.5194/soil-7-585-2021.

Montes, C.R., Lucas, Y., Pereira, O.J.R., Achard, R., Grimaldi, M., Melfi, A.J., 2011. Deep plant-derived carbon storage in Amazonian podzols. Biogeosciences 8, 113–120. https://doi.org/10.5194/bg-8-113-2011.

Montes, C.R., Merdy, P., da Silva, W.T.L., Ishida, D., Melfi, A.J., Santin, R.C., Lucas, Y., 2023. Mineralization of soil organic matter from equatorial giant podzols submitted to drier pedoclimate: a drainage topochronosequence study. Catena (Amst) 222, 106837. https://doi.org/10.1016/j.catena.2022.106837.

Parikh, S.J., Goyne, K.W., Margenot, A.J., Mukome, F.N.D., Calderón, F.J., 2014. Soil chemical insights provided through vibrational spectroscopy. Academic Press Inc., pp. 1–148. https://doi.org/10.1016/B978-0-12-800132-5.00001-8

R Core Team, 2021. R: A Language and Environment for Statistical Computing.

Roth, H.K., Borch, T., Young, R.B., Bahureksa, W., Blakney, G.T., Nelson, A.R., Wilkins, M.J., McKenna, A.M., 2022. Enhanced speciation of pyrogenic organic matter from wildfires enabled by 21 T FT-ICR mass spectrometry. Anal. Chem. 94, 2973–2980. https://doi.org/10.1021/acs.analchem.1c05018.

Roth, V.N., Lange, M., Simon, C., Hertkorn, N., Bucher, S., Goodall, T., Griffiths, R.I., Mellado-Vázquez, P.G., Mommer, L., Oram, N.J., Weigelt, A., Dittmar, T., Gleixner, G., 2019. Persistence of dissolved organic matter explained by molecular changes during its passage through soil. Nat. Geosci. 12, 755–761. https://doi.org/10.1038/s41561-019-0417-4.

Rumpel, C., Kögel-Knabner, I., 2011. Deep soil organic matter—a key but poorly understood component of terrestrial C cycle. Plant and Soil 338, 143–158. https://doi.org/10.1007/S11104-010-0391-5.

Ryals, R., Kaiser, M., Torn, M.S., Berhe, A.A., Silver, W.L., 2014. Impacts of organic matter amendments on carbon and nitrogen dynamics in grassland soils. Soil Biol. Biochem. 68, 52–61. https://doi.org/10.1016/j.soilbio.2013.09.011.

Savory, J.J., Kaiser, N.K., McKenna, A.M., Xian, F., Blakney, G.T., Rodgers, R.P., Hendrickson, C.L., Marshall, A.G., 2011. Parts-per-billion Fourier transform ion cyclotron resonance mass measurement accuracy with a "walking" calibration equation. Anal. Chem. 83, 1732–1736. https://doi.org/10.1021/ac102943z.

Schmidt, M.W.I., Knicker, H., Koè Gel-Knabner, I., 2000. Organic matter accumulating in Aeh and Bh horizons of a Podzol: chemical characterization in primary organo-mineral associations. Org. Geochem. 31, 727–734.

Smith, D.F., Podgorski, D.C., Rodgers, R.P., Blakney, G.T., Hendrickson, C.L., 2018. 21 tesla FT-ICR mass spectrometer for ultrahigh-resolution analysis of complex organic mixtures. Anal. Chem. 90, 2041–2047. https://doi.org/10.1021/acs.analchem.7b04159.

Soong, J.L., Fuchslueger, L., Marañon-Jimenez, S., Torn, M.S., Janssens, I.A., Penuelas, J., Richter, A., 2020. Microbial carbon limitation: the need for integrating microorganisms into our understanding of ecosystem carbon cycling. Glob. Chang. Biol. 26, 1953–1961. https://doi.org/10.1111/gcb.14962.

Stone, E.L., Harris, W.G., Brown, R.B., Kuehl, R.J., 1993. Carbon storage in Florida Spodosols. Soil Sci. Soc. Am. J. 57, 179–182. https://doi.org/10.2136/SSSAJ1993.03615995005700010032X.

United States Department of Agriculture (USDA), 2017. Soil Survey Manual By Soil Science Division Staff, C. Ditzler, K. Scheffe, e H.C. Monger. Government Printing Office, Washington, D.C.

Wagai, R., Mayer, L.M., Kitayama, K., Shirato, Y., 2013. Association of organic matter with iron and aluminum across a range of soils determined via selective dissolution techniques coupled with dissolved nitrogen analysis. Biogeochemistry 112, 95–109. https://doi.org/10.1007/s.

Wilson, R.M., Tfaily, M.M., 2018. Advanced molecular techniques provide new rigorous tools for characterizing organic matter quality in complex systems. Eur. J. Vasc. Endovasc. Surg. https://doi.org/10.1029/2018JG004525.

Xian, F., Hendrickson, C.L., Blakney, G.T., Beu, S.C., Marshall, A.G., 2010. Automated broadband phase correction of Fourier transform ion cyclotron resonance mass spectra. Anal. Chem. 82, 8807–8812. https://doi.org/10.1021/ac101091w.

Ye, Q., Wang, Y.H., Zhang, Z.T., Huang, W.L., Li, L.P., Li, J., Liu, J., Zheng, Y., Mo, J.M., Zhang, W., Wang, J.J., 2020. Dissolved organic matter characteristics in soils of tropical legume and non-legume tree plantations. Soil Biol Biochem 148. https://doi.org/10.1016/j.soilbio.2020.107880.

Zechmeister-Boltenstern, S., Keiblinger, K.M., Mooshammer, M., Penuelas, J., Richter, A., Sardans, J., Wanek, W., 2015. The application of ecological stoichiometry to plant-microbial-soil organic matter transformations. Ecol. Monogr. https://doi.org/10.1890/14-0777.1.

Zsolnay, A., 1996. Dissolved Humus in Soil Waters, in: Humic Substances in Terrestrial Ecosystems. Elsevier, pp. 171–223. https://doi.org/10.1016/B978-044481516-3/50005-0.

Zsolnay, Á., 2003. Dissolved organic matter: artefacts, definitions, and functions. Geoderma 113, 187–209. https://doi.org/10.1016/S0016-7061(02)00361-0.